

## Optical and morphological properties of DCM thin films co-doped of Znq<sub>2</sub> by PVD: Theoretical and experimental investigations

Amina Laouid<sup>a,b,c,\*</sup>, Amine Alaoui Belghiti<sup>b</sup>, Krzysztof Wisniewski<sup>a,c</sup>, Janusz Strzelecki<sup>a</sup>, Asli Karakas<sup>d</sup>, Aysun Gozutok<sup>d</sup>, Youssef El kouari<sup>e</sup>, Amal Bouich<sup>f</sup>, Mouhaydine Tlemçani<sup>g,h</sup>, Przemyslaw Plociennik<sup>c,i</sup>, Abdelowahed Hajjaji<sup>b</sup>, Anna Zawadzka<sup>a,c</sup>

<sup>a</sup> Institute of Physics, Faculty of Physics, Astronomy, and Informatics, Nicolaus Copernicus University in Toruń, Grudziądzka 5, PL 87-100, Toruń, Poland

<sup>b</sup> Chouaib Doukkali University of El Jadida, National School of Applied Sciences, Engineering Science for Energy Lab, El Jadida, Morocco

<sup>c</sup> Centre for Modern Interdisciplinary Technologies, Nicolaus Copernicus University in Toruń, Wileńska 4, PL 87-100, Toruń, Poland

<sup>d</sup> Selcuk University, Faculty of Sciences, Department of Physics, Campus, Konya, Turkey

<sup>e</sup> Laboratory of Materials, Energy and System Control (LMECS), Faculty of Sciences and Technology, Hassan II University of Casablanca, Mohammedia, Morocco

<sup>f</sup> Institut de Disseny i Fabricació, Universitat Politècnica de València, Camí de Vera s/n, 46022, Valencia, Spain

<sup>g</sup> Instrumentation and Control Laboratory, Institute of Earth Sciences, Universidade de Évora, Colégio Luís António Verney, Rua Romão Ramalho, N° 59, 7000-671, Évora, Portugal

<sup>h</sup> Department of Mechatronics Engineering, School of Science and Technology, Universidade de Évora, Colégio Luís António Verney, Rua Romão Ramalho, N° 59, 7000-671, Évora, Portugal

<sup>i</sup> Institute of Engineering and Technology, Faculty of Physics, Astronomy and Informatics, Nicolaus Copernicus University in Toruń, ul. Grudziądzka 5, 87-100, Toruń, Poland

### ARTICLE INFO

Handling Editor: Prof. L.G. Hultman

**Keywords:**

DCM - Znq<sub>2</sub> thin film

PVD

UV-Vis spectroscopy

AFM

Density functional theory

FTIR

TEM

### ABSTRACT

In this article, new experimental results of the morphological and optical properties of thin films of 4-(dicyanomethylene)-2-methyl-6-(4-dimethylaminostyryl)-4H-pyran co-doped by 8-hydroxyquinoline zinc (Znq<sub>2</sub>) for different concentrations were presented. The physical vapor deposition in a high vacuum was used to create the thin films on glass substrates with a thickness of 100 nm. The morphological properties of the samples were identified using the Atomic Force Microscopy (AFM) apparatus in tapping mode. TEM images show amorphous structures. The phase composition of the samples was assessed using FTIR methods. The Tauc plot approach was used to examine the measured transmittance spectra in order to estimate the energy gap. Analysis of the results showed that the co-doping of DCM thin film by Znq<sub>2</sub> influenced the structural and optical properties of the samples. To evaluate the experimental results found, theoretical calculations based on the maximum one-photon absorption (OPA) wavelengths of DCM and Znq<sub>2</sub> have been first measured through the UV-Vis spectral technique. Then, the experimental conclusions on values for DCM and Znq<sub>2</sub> have been compared with their corresponding simulation data procured from the time-dependent self-consistent-field (TD-SCF) computation utilizing the density functional theory (DFT) at B3LYP/6-311G(d,p) level. Besides, we have explored the first and second frontier molecular orbitals (MOs) for title compounds and their energy gaps via the DFT procedure. The calculations of maximum OPA wavelengths and the highest occupied molecular orbital (HOMO) and the lowest unoccupied molecular orbital (LUMO) contributions on both molecules have also been crosschecked with the results of already published data in the literature.

### 1. Introduction

In recent years, organic compounds have appeared awesome potential as appropriate materials for optoelectronic applications [1–5].

Among numerous organic materials, the 4-(dicyanomethylene)-2-methyl-6-(4-dimethylaminostyryl)-4H-pyran (DCM) molecule, being a member of the merocyanine dyes category, has gained particular attention of many applications for being representing a low-cost and

\* Corresponding author. Institute of Physics, Faculty of Physics, Astronomy, and Informatics, Nicolaus Copernicus University in Toruń, Grudziądzka 5, PL 87-100, Toruń, Poland.

E-mail address: [laouidamina9@gmail.com](mailto:laouidamina9@gmail.com) (A. Laouid).

broadband fabric [6]. It was first reported in the 1970s by Webster et al. at the Eastman-Kodak company as a doping material for the improvement of red laser materials. It is a laser dye that has strong absorption in the green and blue regions of the spectrum and when incorporated into a host material, can produce laser light in the red region of the spectrum [7]. Due to its unique photophysical and optoelectronic properties, considerable research has been conducted on the use of DCM in a wide range of applications. In addition to its use in lasers, DCM has been explored for other applications, including organic light emitting diodes (OLEDs) as it exhibits high efficiency and brightness, as well as good color purity [8,9] in photovoltaic applications as an electron acceptor in bulk heterojunction solar cells, where it has shown promising results in improving the device performance [10]. Nonlinear optics (NLO) applications that exhibit high third-order nonlinear optical properties, natural applications to study the photosynthesis process in plants, as it is able to mimic the absorption characteristics of chlorophyll [11], bio-imaging, and sensors as they can be used as fluorescent probes to label biomolecules and cells. Furthermore, DCM has been used as a sensing material, where it has been incorporated into optical fibers and other sensing devices to detect a range of analytes, including pH, temperature, and metal ions [12].

DCM molecule contains an organic  $\pi$ -system, with an electron acceptor (A) and an electron donor (D) [13,14]. The electron acceptor (A) is represented by a dicyanomethylene, while the electron donor (D) is represented by a group N, N-dimethylaniline covalently bound to each other by a conjugated  $\pi$  fragment represented by 4 H-pyran-4-sliding, in the form of an electron donor-acceptor architecture (D- $\pi$ -A), forming with this structure a category of molecules known as push-pull systems [15–17]. This molecule has special properties due to the interactions between the donor and the acceptor [18]. The interaction forms a new low-energy molecular orbital that facilitates electron excitation, the process is called intramolecular charge transfer [19]. It's a highly versatile and widely studied molecule that has gained significant interest in the field of advanced materials sciences. It's simple synthesis, well-defined structure [20], and ability to exhibit high quantum fluorescence efficiency and long lifetime in the excited state have made it a popular choice for a variety of applications [21]. In addition to its optical properties, DCM has also been found to possess excellent thermal and chemical stability, making it suitable for use in harsh environments. Its ability to function as a versatile dopant material for various host matrices has further expanded its potential applications.

According to the reported work, several methods have been used to exploit the interesting properties presented by DCM and to take advantage of the great potential that has been demonstrated in it. It was studied in non-polar solvents [22], bulk solvents, and biological systems [23], as a doping material for thin layers and luminescent nanoparticles incorporated into polymers [24], however, the films deposited in the form of thin layers are considered one of the most decisive techniques [25,26] since they possess in particular physicochemical properties different from those of the massive materials or in solution.

On the other hand, bis(8-hydroxyquinoline) zinc (Znq<sub>2</sub>) is a versatile organic compound that has garnered significant attention in various research fields due to its unique properties and potential applications. Znq<sub>2</sub> belongs to the family of hydroxyquinoline compounds, which are known for their excellent photoluminescence properties and high thermal stability [27]. It has been of great interest for several research in recent years because of its significant fluorescence [28], excellent photoluminescence properties [29], and significant non-linear optical properties. It has shown benefits by comparing it with other materials in terms of its electron transport and its higher quantum efficiency in device performance [30].

Znq<sub>2</sub> is an organic semiconductor with properties similar to inorganic semiconductors [31]. Due to its mechanical, thermal, and chemical properties, Znq<sub>2</sub> has been the subject of a strong interest in a variety of applications, including electronics, photographic electronics, optoelectronics, medicine, bioanalytical science, agriculture, and especially

for organic LEDs [32]. This type of material has also contributed to the creation of organic plastic and electronics.

Until recently, various physical and chemical techniques were used to grow thin films of DCM and thin films of Znq<sub>2</sub> separately. In this work, we report for the first time a new composition of thin films based on DCM and Znq<sub>2</sub> molecules with different percentages of Znq<sub>2</sub> inside the samples (10%, 30%, 50%, 80%, 90%, and 95%). The reason for selecting the specific percentages of Znq<sub>2</sub> in the co-deposition process is to investigate the influence of Znq<sub>2</sub> on the optical properties of DCM red dye. The use of different percentages allows for the creation of a series of thin films with varying amounts of Znq<sub>2</sub>, which can be used to establish a correlation between the amount of Znq<sub>2</sub> and the optical properties of the films. The prepared thin films were deposited using the Physical Vapor Deposition (PVD) method. The objective of this work is to study the influence of co-doping with different percentages of Znq<sub>2</sub> on the structural and optical properties of DCM thin films. In order to interpret and validate the experimental results, a quantum chemical calculation was performed using DFT investigation. The computations of OPA wavelengths defined to the lowest lying electronic transitions, HOMO, and LUMO energies (for first and second frontier MOs) have been executed by TD-SCF/DFT/B3LYP procedure. The calculated outcomes for OPA wavelengths of DCM and Znq<sub>2</sub> have been checked with the measurement data acquired from UV-Vis spectral analyses. The utilized computational chemistry implicating the DFT method is an effectual medium to confirm the structure-property affair of title materials. So, it is immediately required to computationally plan and explore different kinds of organic semiconductors revealing susceptible HOMO-LUMO energy gaps and  $\lambda_{\max}$  results in optoelectronic technics.

## 2. Experimental methods

### 2.1. Deposition of thin films

The thin layers of pure and DCM-doped Znq<sub>2</sub> were deposited on a glass substrate by the Physical Vapor Deposition (PVD) method. The DCM and Znq<sub>2</sub> powders were purchased from Sigma-Aldrich and used as received without any further purification.

The deposition process was performed using a vacuum system called the thin film Deposition System - NANO 36<sup>TM</sup> (Kurt J. Lesker Company) [33–35]. The deposit is made inside the vacuum chamber, shown in Fig. 1, under the pressure of about  $1.3 \times 10^{-6}$  mbar. This vacuum was created using a vacuum system consisting of a rotary pump RP and diffusion pump DP. The primary vacuum is created by using the rotary pump, which has the following characteristics: rotation speed = 1500 tr/mm, pumping speed = 9 m<sup>3</sup>/h, and max. gas throughput = 2722 hPa l/s. The secondary vacuum is generated by using the DP pump, which has a speed of pumping 1200 l/s for Air, and 1500 l/s for Helium with max throughput = 2,5 l/s at 13.3 Pa. The principle of this method is generally based on four essential steps. First, a transformation of the material deposited in the vapor phase by evaporation, then the transfer of atoms (or molecules) from the evaporation source to the substrate on almost rectilinear trajectories, since we work under a very deep vacuum, then the deposition of these particles on the substrate and finally the growth of the film or layer. The thickness of the deposited layer will depend on the evaporation rate, source geometry, substrate of the evaporation time, and distance between substrates and source. DCM and Znq<sub>2</sub> powders have been placed on two different crucibles as shown in Fig. 1 and the distance between them and the glass substrates is equal to 20 cm. Since we want to deposit different compositions, the crucibles have been covered up to the control of the desired rate, then we are open to start deposition. During the entire deposition process, the substrates rotated at a speed of 20 rot/min, while the film thicknesses and deposition rates were controlled by piezoelectric detectors (Fig. 1). The deposition process stops automatically when the desired thin film thickness is obtained. The thin film thickness was determined by the vacuum system using a piezoelectric detector.

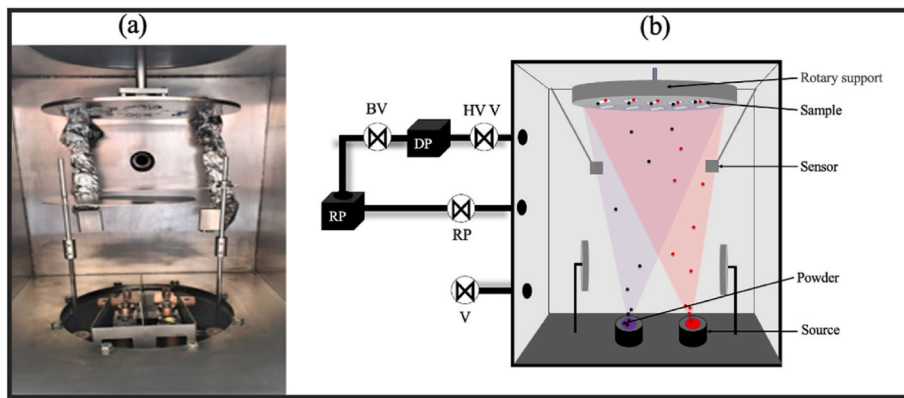


**Fig. 1.** Vacuum chamber of the PVD apparatus (a), diagram of the co-deposition vacuum evaporation process (b),  $V_{1,2,3,4}$  valves, RP; rotary pump, DP; diffusion pump.

## 2.2. Characterization of thin films

In order to visualize the surface texture and qualitatively measure the surface roughness of the thin films of DCM co-doped  $Znq_2$ , atomic force microscopy (AFM) analyses were performed. The AFM measurements were achieved by Keysight 5500, with PPP-NCST cantilevers from Nanosensors equipment in tapping mode. The AFM data were examined using the Gwyddion software [36] based on the calculation of Minkowski (MF) functions. The Minkowski functions are based on the calculation of different parameters, the discrete two-dimensional variants of volume  $V$ , surface  $S$ , and connectivity (characteristic of Euler-Poincaré)  $\chi$  to describe the overall geometric characteristics of the film structures [37, 38].

A double-beam spectrophotometer (Perkin Elmer Lambda 2 UV/VIS/NIR) was also used to measure the transmission spectra at normal incidence in the spectral range 190–1100 nm.

Fourier transform infrared (FTIR) spectrum in region 200–4000  $\text{cm}^{-1}$  was obtained using Bruker alpha spectrometer.

Transmission electron microscopy (TEM)(JEOL-JEM-1010) analysis was carried out with 2.5 kV at different magnifying tools. Field Emission Transmission Electron Microscope of 200 kV (TEM 200).

## 3. Results and discussion

### 3.1. Morphological properties

Fig. 2 shows the bi and three-dimensional AFM images of all the prepared samples. The surfaces studied are equal to  $1 \times 1 \mu\text{m}$  of the surface.

The AFM observations clearly show that there is a remarkable change in the morphology and roughness of the surface of the DCM film as a function of the percentage of  $Znq_2$  inside the sample. By increasing the percentage of  $Znq_2$  inside the sample, the structure of the film develops towards a more or less sponged structure at low thickness, the grains start to disappear and the structure begins to create agglomerate which was particularly remarkable. For example, it is clearly demonstrated from the sample of 10%DCM-90% $Znq_2$  that the structure of  $Znq_2$  is the most dominant. Conversely, as the percentage of  $Znq_2$  decreases, grain size also increases, with rough surfaces that can be clearly seen in 3D AFM images (Fig. 2). For large percentages of DCM, as in the case of the sample 90%DCM-10% $Znq_2$ , the morphology of the film develops into a structure which grains of elliptical shape. The sample with 50% DCM-50% $Znq_2$  shows that the structure is well deposited and the equitable presence of both materials can be observed.

The roughness of the surface is an important factor to consider since it influences the properties of the thin layer [39]. One of the dispersion factors used to characterize surface roughness is the root mean square

roughness ( $S_q$ ), which is calculated by squaring each dataset's height value and then finding the square root of the mean.

It has been reported that doping DCM with  $Znq_2$  can introduce lower average crystallite size, which can reduce film surface roughness. Table 1 groups collectively the roughness values for all samples. According to Table 1, the integration of the dopant in the DCM films affects the surface and decreases the average size of the grains; however, mean square roughness (RMS) reduced as  $Znq_2$  dopant levels rose. However, by analyzing the functions of Minkowski  $V(z)$ ,  $S(z)$ , and  $\chi(z)$  it is possible to confirm the influence of the co-doping on the structural properties of thin films of DCM. For the Minkowski surface curves, as shown in Fig. 3, for all samples the curves increase fast to the maximum value which differs according to the percentage of  $Znq_2$  in the film composition, then go fast to zero, except for the film with composition 90%DCM-10% $Znq_2$ , the curve decreases to a local minimum then approaches zero. All samples of the Minkowski surface curves are more or less the same, except for the films 50%DCM-50% $Znq_2$  and 90%DCM-10% $Znq_2$  they are a little out of step concerning the others and they have the highest and lowest values for the maximums respectively. In addition, Fig. 4 represents the Minkowski connectivity curves which take either positive or negative values. The negative values indicate that the surface is porous in this case we have the predominance of the valleys. In contrast, positive values represent punctiform structures. moreover, the maximum values represent the densest peaks, while the minimum corresponds to the highest density of valleys. As Fig. 5 proves, for all samples, the Minkowski volume curves remain flat at the beginning and then fall to zero.

### 3.2. Transmission Electron Microscopy (TEM)

Transmission Electron Microscopy (TEM) is a powerful technique used to image the internal structure of thin samples at a very high resolution [40]. It involves transmitting a beam of high-energy electrons through the sample to form an image, providing detailed information about the morphology and structure of materials at the nanoscale [41, 42].

In the study, TEM result revealed that all the samples with different percentages of red dye (DCM) and the zinc (II) bis(8-hydroxyquinoline) ( $Znq_2$ ) complex formed a non-crystalline, amorphous structure in the thin films. Fig. 6 depicts an example of image samples with percentages of 20 %, 50%, and 70% of DCM in the structure.

This amorphous phase is a common characteristic of thin films deposited by Physical Vapor Deposition, where the high energy of the deposited material and rapid cooling rate can lead to the formation of non-crystalline structures [43, 44]. The combination of the materials or their interaction, such as DCM and  $Znq_2$ , may also contribute to the amorphous phase formation. The rapid cooling during the PVD process

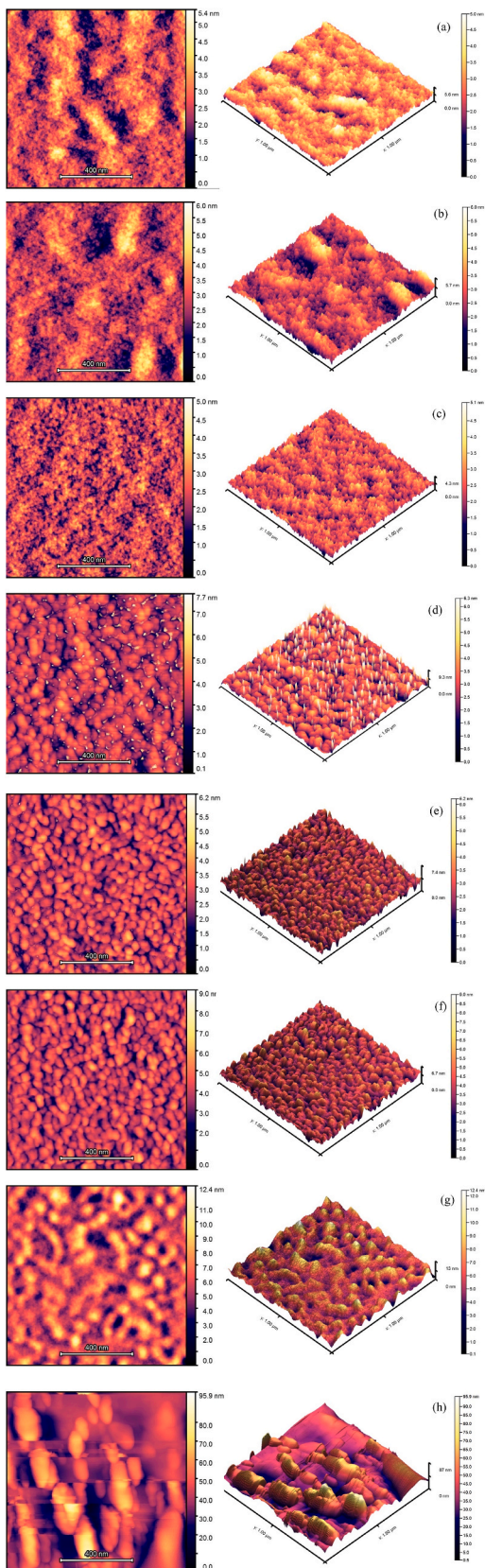


**Fig. 2.** 2D and 3D atomic force microscope (AFM) images ( $1 \mu\text{m} \times 1 \mu\text{m}$ ) of DCM thin films doped: (a) 5%DCM-95%Znq<sub>2</sub>, (b) 10%DCM-90%Znq<sub>2</sub>, (c) 20%DCM-80%Znq<sub>2</sub>, (d) 50%DCM-50%Znq<sub>2</sub>, (e) 70%DCM-30%Znq<sub>2</sub>, (f) 90%DCM-10%Znq<sub>2</sub>, (g) Pure Znq<sub>2</sub> and (h) Pure DCM.

**Table 1**

The values of roughness (RMS) and the average value for all the studied samples.

	RMS roughness (Sq) (pm)	Average value (nm)
5%DCM- 95%Znq <sub>2</sub>	653.02	2.24
10%DCM-90%Znq <sub>2</sub>	669.46	2.71
20%DCM-80%Znq <sub>2</sub>	501.84	2.14
50%DCM-50%Znq <sub>2</sub>	711.13	2.56
70%DCM-30%Znq <sub>2</sub>	548.61	2.71
90%DCM-10%Znq <sub>2</sub>	824.54	3.66
Pure Znq <sub>2</sub>	1.57 (nm)	6.94
Pure DCM	11.48 (nm)	39.82

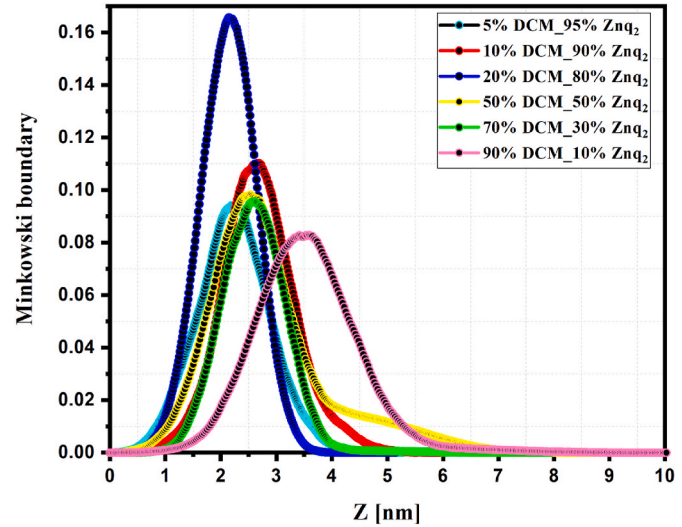


**Fig. 3.** The Minkowski surface  $S(z)$  [no unit] for the scanning areas of  $1 \mu\text{m} \times 1 \mu\text{m}$  for all the samples.

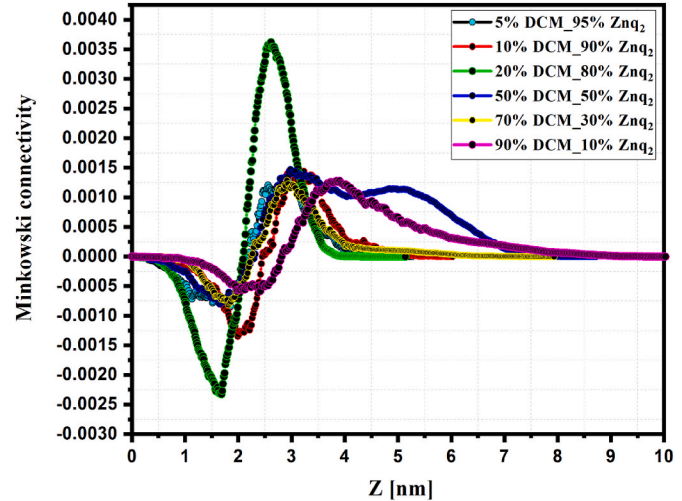


**Fig. 4.** The Minkowski connectivity  $\chi(z)$  [no unit] for the scanning areas of  $1 \mu\text{m} \times 1 \mu\text{m}$  for all the samples.

can prevent the material from forming a crystalline structure, resulting in the observed amorphous phase. This information provides valuable insights into the structural properties of the thin films and the influence of the deposition process and material interactions on their characteristics [45].

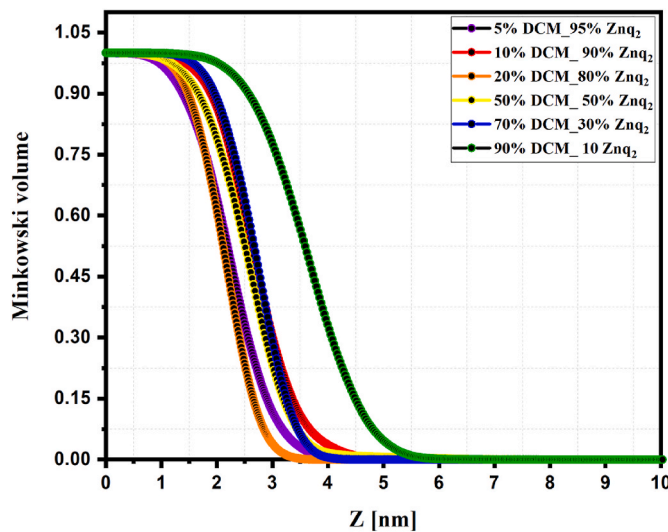


**Fig. 5.** The Minkowski volume  $V(z)$  [no unit] for the scanning areas of  $1 \mu\text{m} \times 1 \mu\text{m}$  for all the samples.

### 3.3. Optical properties

The absorbance  $A(\lambda)$  of the samples of DCM deposited with different percentages of  $\text{Znq}_2$  is shown in **Fig. 7**. The measurement was performed in the  $190\text{--}1100\text{ nm}$  spectral range at normal incidence and room temperature. It can be noted that all the compounds studied are capable of absorbing the light from  $200\text{ nm}$  to about  $600\text{ nm}$ , that is to say in the

UV range and a part of visible, in which the sharp peaks are observed at  $465\text{ nm}$  and the intensity of these peaks depends heavily on the percentage of  $\text{Znq}_2$ . As the percentage of  $\text{Znq}_2$  increased, the absorbance of the samples is reduced. The sample of pure  $\text{Znq}_2$  absorbs the light from  $250\text{ nm}$  at about  $465\text{ nm}$  and it has the lowest absorbance. On the other hand, the sample of pure DCM absorbs light in a wide range from  $250\text{ nm}$  to  $1100\text{ nm}$ , however, the strongest absorbance is between  $250\text{ nm}$  and  $600\text{ nm}$ .

The transmittance of the thin films studied was measured in a wavelength range from  $250\text{ nm}$  to  $1100\text{ nm}$  using the same machine used in the case of absorbance. **Fig. 8** shows the transmittance curves of the thin layers of the studied compounds. The spectrum can be partitioned into three main regions. The first region, where the transmission is low and the films are considered light absorbers, is in the waveband from  $250\text{ nm}$  to  $400\text{ nm}$ . The second region is more absorbent than the first, and is in the waveband from  $400\text{ nm}$  to  $600\text{ nm}$ , in this region, samples with different percentages have a new response. This response represents a feature that does not exist in pure DCM and pure  $\text{Znq}_2$  samples. It can be reported that these compounds have characteristic peaks of low transmittance whose intensity depends on the sample composition, the net peaks are observed at  $465\text{ nm}$ . This behavior can be explained by the possibility of band formation due to the combination of these two organic materials (DCM and  $\text{Znq}_2$ ) during deposition. While the third region where the transmittance is greater is within the wavelength range of  $560\text{ nm}$ – $1100\text{ nm}$ . The transmittance spectrum clearly shows that doping improves transmittance even with small percentages as in the case of  $90\%\text{DCM-10\%Znq}_2$  film. In particular, the form of transmittance spectra of thin films of the studied compounds approximated the superimposition of the transmittance spectrum of pure DCM

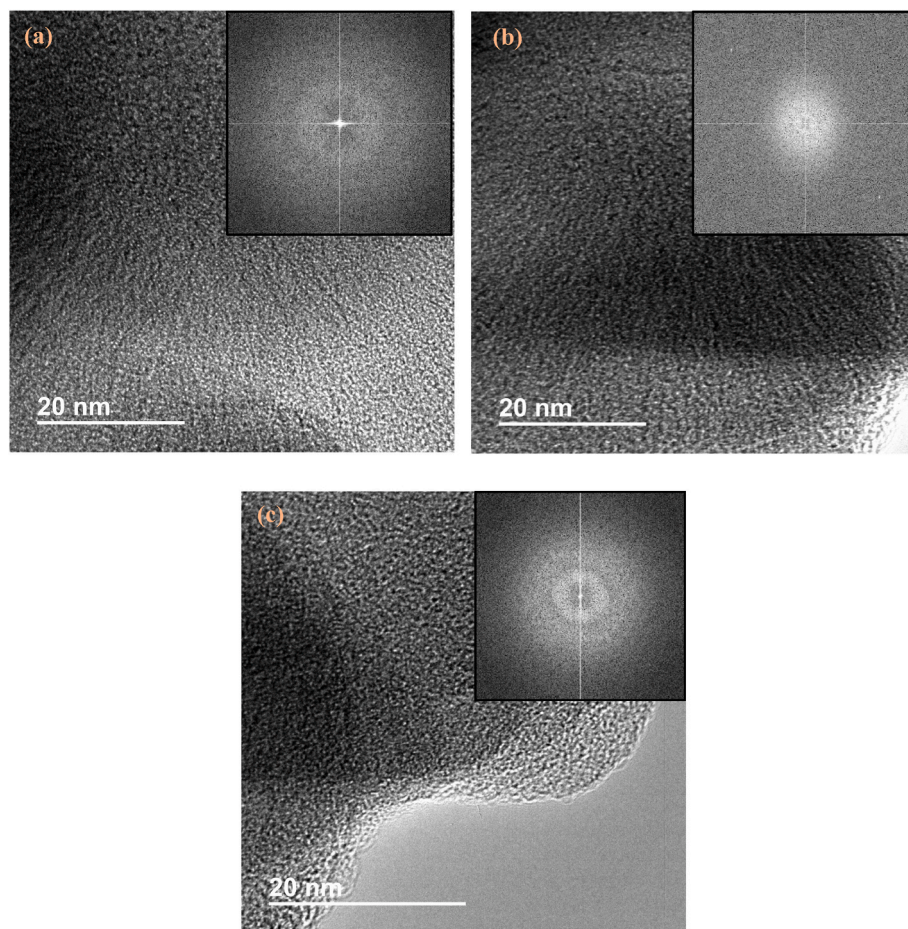


**Fig. 6.** TEM images of: (a)  $20\%\text{DCM-80\%Znq}_2$ , (b)  $50\%\text{DCM-50\%Znq}_2$ , and (c)  $70\%\text{DCM-30\%Znq}_2$  thin films.

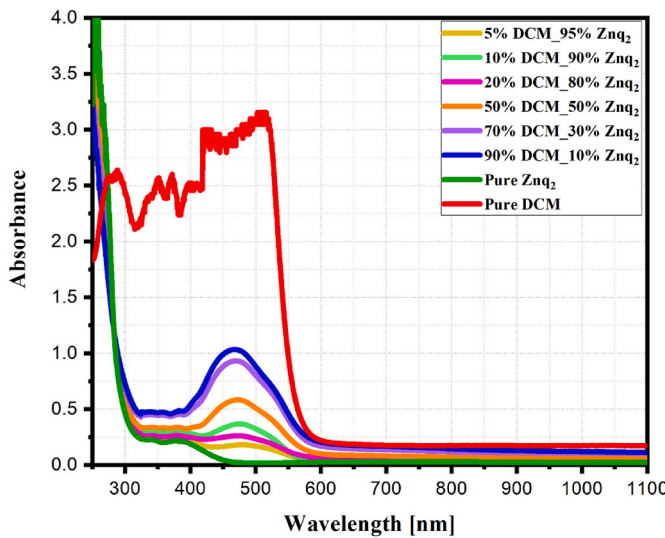


Fig. 7. Absorbance spectra of DCM thin films with different percentages of Znq<sub>2</sub>.

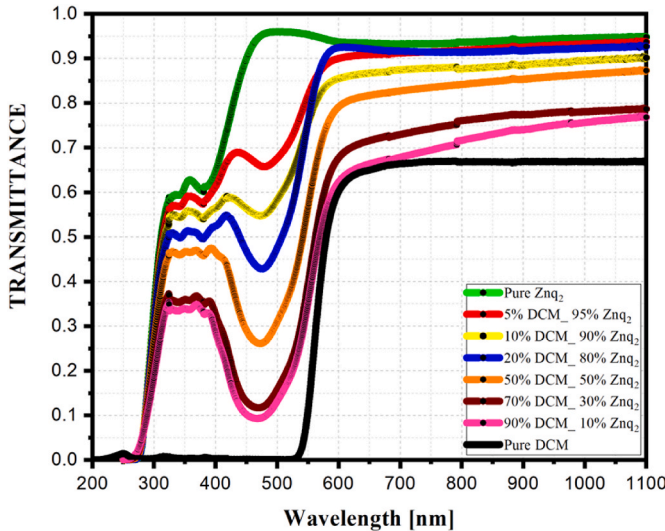


Fig. 8. The transmittance spectra of DCM thin films with different percentages of Znq<sub>2</sub>.

and pure Znq<sub>2</sub> samples. The transmittance intensity of the thin films of the studied compounds was considered to be dependent on the concentration of Znq<sub>2</sub> in the sample, as shown in Fig. 8. For example, the sample 90%DCM-10%Znq<sub>2</sub> has a lower transmittance peak and therefore a large absorbance, and as the percentage of Znq<sub>2</sub> increases, the transmittance also increased.

To determine the most important parameters of the semiconductor thin layers incarnate in the optical transition type and the optical bandwidth ( $E_g$  which represents the gap between HOMO and LUMO energy levels), the Tauc plot remains the most frequently used method [46]. The principle of this method is based on the use of optical absorbance data [47]. The analysis of the absorbance spectrum as a function of the energy of the photons near the area of the absorption edge makes it possible to determine these parameters using the following equation [48];

$$(\alpha h\nu)^{1/m} = \alpha_0(E - E_g) \quad (1)$$

Where  $h$  is Planck constant,  $\nu$  is the photon frequency,  $\alpha$  is the absorption

coefficient,  $\alpha_0$  is a constant of proportionality,  $E_g$  is the gap energy and  $m$  is the exponent value.

Through the value of  $m$ , we can determine the type of electronic transition (between HOMO and LUMO) [49] ( $m = 1/2$  direct allowed transitions,  $m = 3/2$  direct forbidden transitions,  $m = 2$  indirect allowed transitions, and  $m = 3$  indirect forbidden transitions

The absorption coefficient was calculated across the transmittance spectrum and the thickness of the film was based on the following relationships [50,51]:

$$\alpha = A/0.4343 * d \quad (2)$$

$$A = -\log(T) \quad (3)$$

In this work, we have plotted the  $(\alpha h\nu)^{1/m}$  as a function of  $(h\nu)$  and we have made Extrapolation of the linear part of the curves to the point where  $(\alpha E)^m = 0$  to indicate the value of  $E_g$ .

This calculation was performed for different values of  $m$  and the best fit found provided for  $m = 1/2$ .

Fig. 9 represents the Tauc plots for the different studied compositions. Table 2 represents all gap energies for all the studied samples.

The analysis of the results presented in Fig. 9 and Table 2 shows that all samples have several energy gaps. The pure DCM sample (Fig. 9, (a)) showed 4 energy gaps in 2.2 eV, 3 eV, 3.13 eV, and 3.5 eV. The first transition in 2.2 eV, is most probably related to the fundamental transition between HOMO-LUMO, this result is in agreement with the data reported by Fujii and all [52], while the estimated theoretical gap energy of DCM by DFT analysis is 3 eV [53] and the other energy gap transitions are associated to the energy level trapped inside the HOMO-LUMO space.

However, the pure Znq<sub>2</sub> sample has shown the presence of 3 energy gaps (Fig. 9, (b)) in 2.8 eV, 3.14 eV, and 3.42 eV. The first energy gap in 2.8 eV is an energy gap found by the majority of the experimental works [54], while the energy gaps in 3.42 eV and 3.14 eV are the value found by DFT calculations [55]. The pure DCM and pure Znq<sub>2</sub> films showed two energy gaps in the same position (3.14 eV and 3.5 eV).

The samples with different compositions deposited on the glass substrates showed 5 energy gaps (Fig. 9, (c),(d),(e),(f),(g), and (h)). They showed the characteristic energy gaps of pure DCM 2.2 eV and 3.5 eV and also the characteristic energy gaps of pure Znq<sub>2</sub> 2.8 eV and 3.4 eV. However, it is noted the absence of the energy gaps of 3.14 eV and 3 eV, while the presence of the two new energy gaps has been highlighted.

As it is known the DCM molecule belongs to the push-pull system which has both an electron donor group and an electron acceptor group. And the Znq<sub>2</sub> molecule has been used in several research as an electron donor molecule [56], so the combination of these two molecules will produce a donor1-acceptor-donor2 architecture system, as shown in Fig. 10. The interaction between donor1-acceptor produces the first adsorption energy gaps at 2.2 eV which are attributed to the direct transition within DCM. In contrast, the second adsorption at 2.82 eV corresponds very well to the transition within Znq<sub>2</sub>. The new energies at  $2.53 \pm 0.05$  eV and 2.63 eV are most likely due to the transition in the new structure created by the Van der Waals interaction between acceptor-donor2.

In particular, we deposited the two materials without destroying their structures by controlling several parameters, these can be evidenced by the presence of molecules of pure Znq<sub>2</sub> and pure DCM indicated by their gap energy, and also the images of the AFM, more precisely 50%DCM-50%Znq<sub>2</sub>, the film showed that the deposited structure consists of a joint of the molecules DCM-Znq<sub>2</sub> assembled in a common way forming the structure of the sample which may confirm this hypothesis.

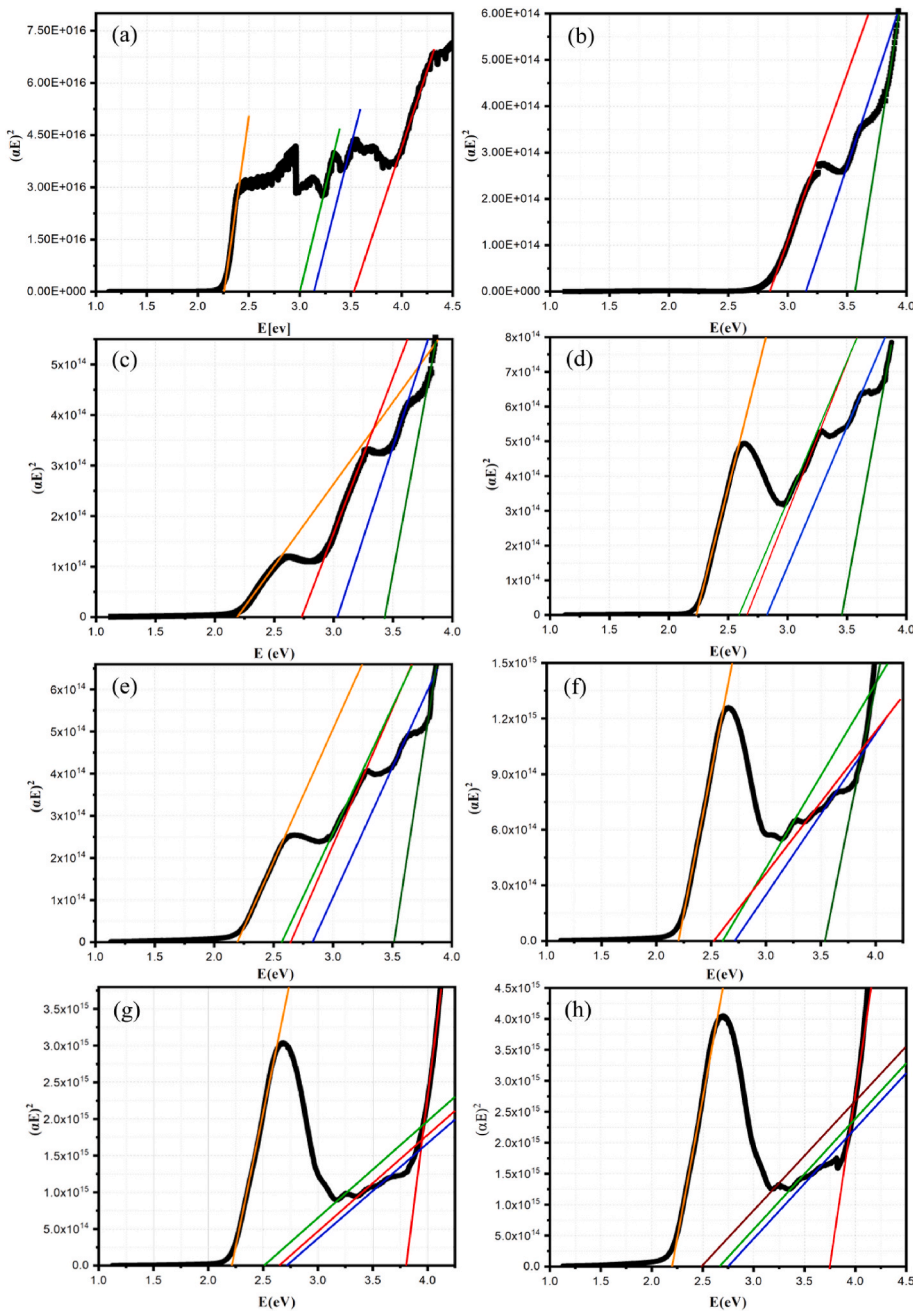


**Fig. 9.** Energy gap determination plots of (a) Pure DCM, (b) Pure Znq<sub>2</sub>, (c) 5%DCM- 95%Znq<sub>2</sub>, (d) 10%DCM- 90%Znq<sub>2</sub>, (e) 20%DCM- 80%Znq<sub>2</sub>, (f) 50%DCM- 50% Znq<sub>2</sub>, (g) 30%DCM-70%Znq<sub>2</sub> and (h) 10%DCM-90%Znq<sub>2</sub> thin films.

**Table 2**

The table groups the values of gap energies obtained by the tauc plot method for all samples.

Gap energy Thin films	$E_g$ (eV)						
	$E_{g1}$	$E_{g2}$	$E_{g3}$	$E_{g4}$	$E_{g5}$	$E_{g6}$	$E_{g7}$
Pure Znq <sub>2</sub>	—	—	—	2.8	3.14	3.42	
Pure DCM	2.2	—	—	3	3.13	3.5	
DCM 5%_Znq <sub>2</sub> 95%	2.2	—	—	2.73	3	—	3.45
DCM 10%_Znq <sub>2</sub> 90%	2.2	2.58	2.65	2.82	—	—	3.45
DCM 20%_Znq <sub>2</sub> 80%	2.2	2.57	2.64	2.82	—	—	3.5
DCM 50%_Znq <sub>2</sub> 50%	2.2	2.51	2.62	2.73	—	—	3.52
DCM 70%_Znq <sub>2</sub> 30%	2.21	2.51	2.64	2.72	—	—	3.7
DCM 90%_Znq <sub>2</sub> 10%	2.2	2.48	2.65	2.73	—	—	3.7

### 3.4. Infrared absorption spectroscopy (FTIR)

The FTIR spectra of studied thin films illustrated in Fig. 11 were utilized to determine the compositions. Based on the spectroscopic data of the sample of pure Znq<sub>2</sub>, the observed vibrations at 1590 and 1327  $\text{cm}^{-1}$  were assigned to the quinoline group of Znq<sub>2</sub>, as reported in Refs. [57,58]. Additionally, the bands detected at 1504 and 1458  $\text{cm}^{-1}$  are attributed to the vibrations of the pyridyl and phenyl groups in Znq<sub>2</sub>. Furthermore, the C–O stretching vibration is responsible for the peak observed at 1108  $\text{cm}^{-1}$ . The C–H deformation vibrations, on the other hand, are associated with the peaks located at 825, 780, and 770  $\text{cm}^{-1}$ . Finally, the peaks at 405  $\text{cm}^{-1}$  are linked to the Zn–O and Zn–N stretching vibrations [59–61]. whereas a distinctive peak centered at approximately 2210  $\text{cm}^{-1}$  in the spectrum of pure DCM is typically attributed to the C–N stretching vibration and the pics detected at 1650

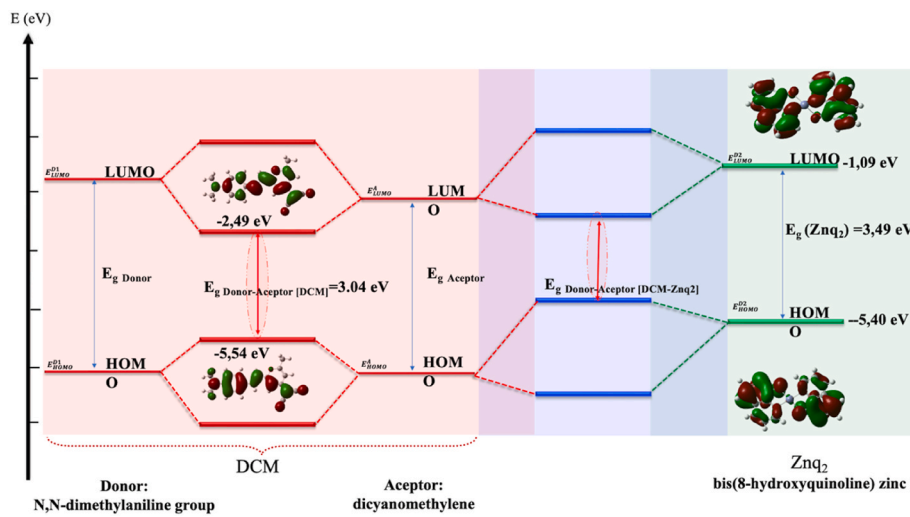


Fig. 10. Energy level diagram of a donor-acceptor-donor system.

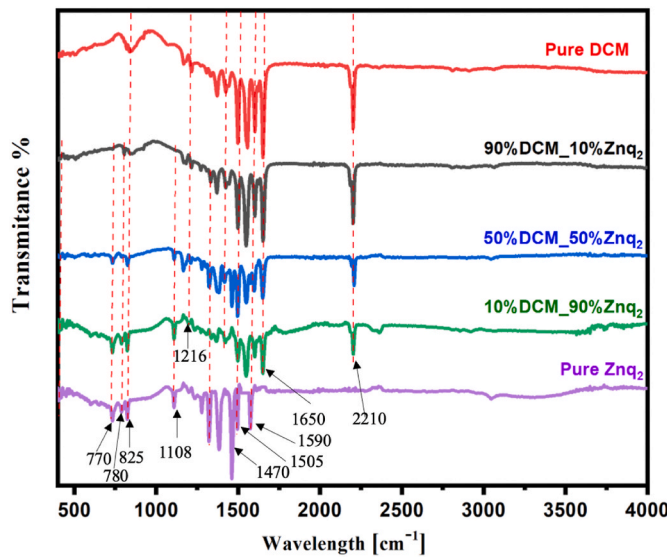


Fig. 11. FTIR spectrums.

and  $1590\text{ cm}^{-1}$  are attributed to the stretching vibration of the  $\text{C}=\text{C}$  bond in the aromatic ring [62,63]. Furthermore, the band at  $1470\text{ cm}^{-1}$ , corresponds to the in-plane bending vibration of the aromatic ring. The observed band at  $1216\text{ cm}^{-1}$ , corresponds to the stretching vibration of the  $\text{C}-\text{O}-\text{C}$  group, and the band at  $820\text{ cm}^{-1}$ , corresponds to the out-of-plane bending vibration of the aromatic ring. Wille distinctive bands are corresponding to the pure forms of ZnS and DCM are observed in the spectra of samples with varying compositions. Further supporting the conclusion that the deposited thin films are pure.

#### 4. DFT investigation

Initially, the studies of geometry optimization have been implemented on the examined semi-conductor materials. The GAUSSIAN03W [64] program at the DFT/B3LYP level with 6-311G(*d,p*) polarized basis set has been exploited to realize the geometrical optimizations. For projecting the molecular structure shapes of DCM and Znq<sub>2</sub>, we have run the GAUSSVIEW03W [65] program which is the interface software of GAUSSIAN03W [64]. The yields on the DFT procedures have been extensively researched in the literature [66]. The B3LYP function is recognized as one of the most suitable processes to reproduce the

molecular structure and linear optical phenomena for organic and organometallic patterns. This functional is constantly operated to constitute sensible experimental trends [67,68]. In this work, to designate the OPA wavelengths ( $\lambda_{\max}$ ) enclosed in the lowest-lying electronic transitions of DCM and Znq<sub>2</sub>, we have chosen to employ the TD-SCF/DFT/B3LYP approach with 6-311G(*d,p*) polarized basis set of the GAUSSIAN03W [64] program. Additionally, to comprehend the concern between linear optical treatment and molecular structure properties; the HOMOs, LUMOs, and HOMO-LUMO energy gaps values have been ensured using the GAUSSIAN03W [64] program at TD-SCF/DFT/B3LYP level using 6-311G(*d,p*) basis set. The energy gap ( $E_g$ ) of first and second frontier MOs is stated as follows [69]:

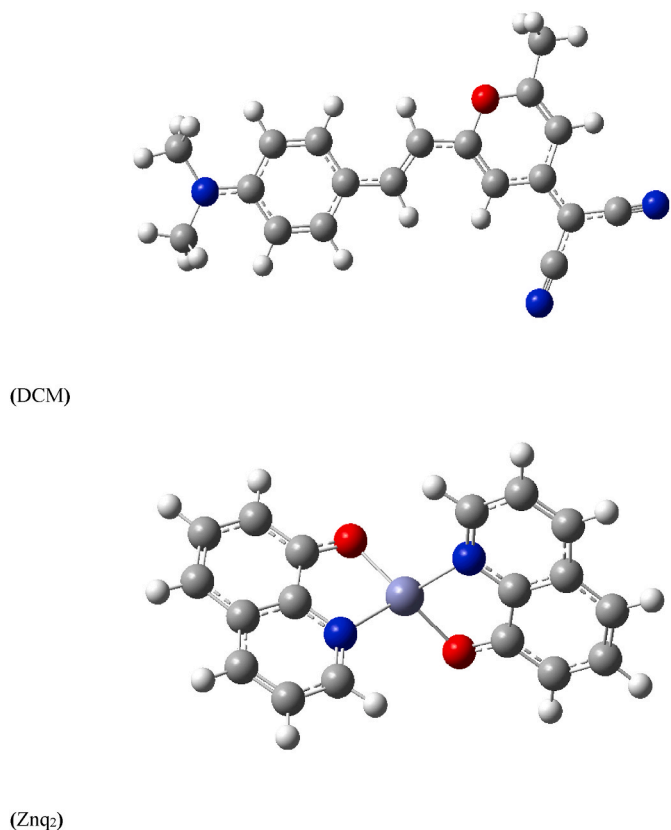
$$E_g = E_{\text{LUMO}} - E_{\text{HOMO}} \quad (4)$$

The geometrically optimized structures computed by the DFT/B3LYP procedure for DCM and Znq<sub>2</sub> are shown in Fig. 12.

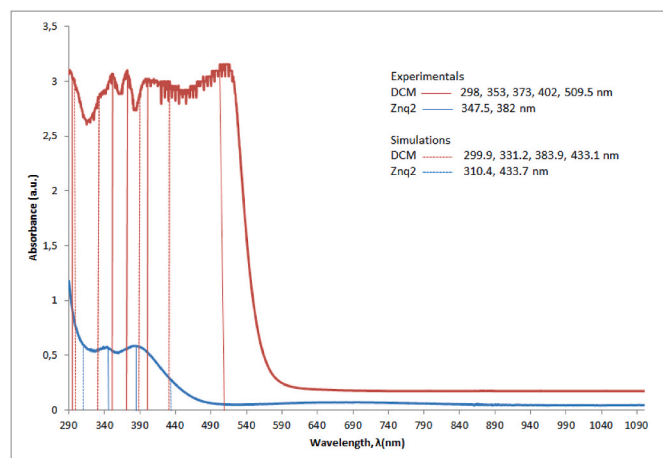
The maximum OPA wavelengths of DCM and Znq<sub>2</sub> have been resolved in the area of 200–1100 nm via UV–Vis recording spectrophotometer. It has been ascertained that DCM and Znq<sub>2</sub>, respectively, have five maximum absorption bands in the domain of 298–510 nm of UV–Vis field (for DCM) and two maximum absorption bands at almost 348 and 382 nm in the UV field (for Znq<sub>2</sub>) as demonstrated in Fig. 13. Further, the UV–Vis absorption spectra have been computationally achieved, representing the vertical transition energies from ground to excited situations. Fig. 13 also illuminates the simulation consequences for OPA wavelengths. The theoretically devised  $\lambda_{\max}$  values of title compounds have pretty well complied with their corresponding measurement conclusions. It is realized from Fig. 13 that the computed results on  $\lambda_{\max}$  values are a little higher (discrepancy within 51 nm at most) and lower (discrepancy within 76 nm at most) than the measured data. Besides, to acquire some comprehension of the MO properties, the HOMO and LUMO energies of DCM and Znq<sub>2</sub> have been analyzed.

Table 3 tabulates the calculated outcomes on first and second frontier MO energies and their energy gaps for DCM and Znq<sub>2</sub>, indicating that data of  $E_g$  [HOMO–LUMO] predicted by DFT procedure in Table 3 match with the experimental values in Table 2 (3 eV, 3.13 eV, 3.5 eV for pure DCM and 3.14 eV, 3.42 eV for pure Znq<sub>2</sub>) well. Fig. 13 elucidates the layouts of all produced MOs. The computed absorption wavelengths, oscillator strengths, and major contributions belonging to the electronic transitions of both examined compounds are listed in Table 4.

The DCM and Znq<sub>2</sub> possess intense simulated major absorption peaks centered at  $\lambda_{\max} = 299.9, 331.2, 383.9, 433.1$  nm (for DCM) and  $\lambda_{\max} = 310.4, 433.7$  nm (for Znq<sub>2</sub>) with relatively high oscillator strengths  $f = 0.2829, 0.1088, 0.0708, 1.1065$  (for DCM) and  $f = 0.0134, 0.0636$  (for



**Fig. 12.** Molecular models of 4-(dicyanomethylene)-2-methyl-6-(4-dimethylaminostyryl)-4H-pyran (DCM) and 8-hydroxyquinoline zinc (Znq<sub>2</sub>). C, N, H, O, and Zn atoms correspond to grey, blue, white, red, and purple ball-shaped, respectively.



**Fig. 13.** UV-Vis absorption spectra as thin film and IR spectrum computed via frequency calculations at the same B3LYP/6-311G(d,p) corresponding to UV-Vis spectra of DCM and Znq<sub>2</sub>.

Znq<sub>2</sub>). On the other hand, the one computed extra peak of DCM at 296.6 nm and three computed extra peaks of Znq<sub>2</sub> at 408.6, 408.9, and 429.8 nm are unavailable in the spectrum owing to the excessively low f values (see Table 4 and Fig. 13).

Meyer et al. [70] viewed the maximum absorption wavelengths of DCM in cyclohexane at 451 and 340 nm. The measurement conclusions on values reported by Ref. [70] are near to both our measured (509.5 and 402 nm) and also simulated (433.1 and 383.9 nm) results depicted in Fig. 13. The DCM carrying pyranylidene malononitrile group

**Table 3**

The calculated first (HOMO, LUMO) and second ((HOMO-1), (LUMO+1)) frontier MO energies and energy gaps in eV unit using the DFT method at B3LYP/6-311G(d,p) level for DCM and Znq<sub>2</sub>.

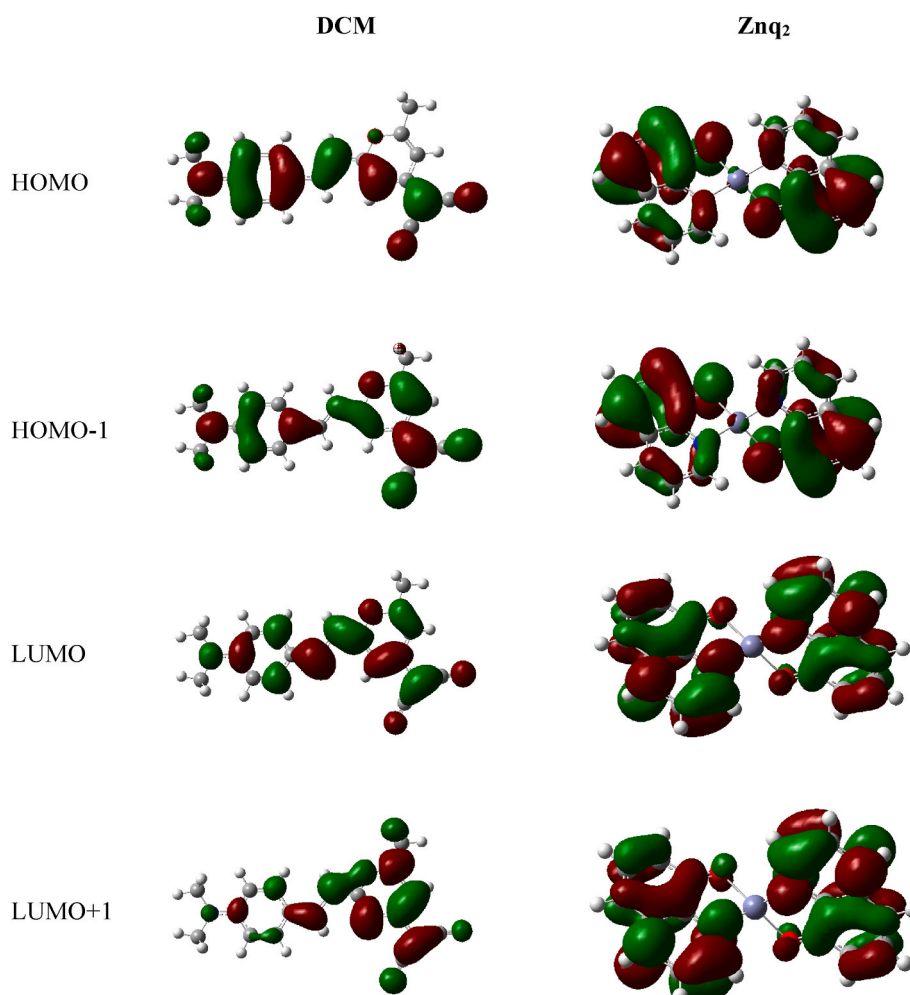
	DCM	Znq <sub>2</sub>
HOMO	-5.54513	-5.40445
LUMO	-2.49691	-1.90670
$E_g$ [HOMO - LUMO]	3.04822	3.49775
HOMO-1	-6.07984	-5.40772
LUMO+1	-1.54533	-1.86779
$E_g$ [(HOMO-1) - (LUMO+1)]	4.53451	3.53993

(electron accepting) and 4-aminostyryl group (electron donating) could be excited by means of UV light at about 400 nm wavelength to generate a locally excited condition from local excitation of electron-accepting group [71]. It might be predicted that this excitation theoretically coincides to HOMO-1 → LUMO transition [71]. It is seen from Table 4 that our calculated maximum absorption wavelengths for DCM at 383.9 and 331.2 nm (corresponding three measured data at 402, 373, 353 nm) contribute to the excitations introduced from UV light at nearly 400 nm, including HOMO-1 → LUMO contributions above mentioned in Ref. [71]. Besides, in this work, the  $\lambda_{max} = 299.9$  nm value (298 nm measured data) corresponding to the fourth singlet excited state of the absorption spectrum for DCM has been observed as an additional peak not determined in the literature [70]. As shown in Fig. 14, the HOMO for DCM has been commonly situated on the electron donating group (4-aminostyryl), whereas the HOMO-1 and LUMO have been mostly deployed on the electron accepting group (pyranylidene malononitrile). In this way, the HOMO → LUMO transmission induces charge transfer (CT) from the donor group to the acceptor group, carving out the intramolecular charge transfer (ICT) situation; and the HOMO-1 → LUMO transmission follows to local excitation of the acceptor group (pyranylidene malononitrile) formed the locally excited (LE) situation. The electron intensity for LUMO+1 of DCM is delivered around the pyranylidene malononitrile moiety (see Fig. 14). Confronted to the published literature, it is tolerably explicit that the first and second frontier MO contributions of DCM in Fig. 14 are properly close to the achieved data in Ref. [72]. The HOMO-LUMO gap ( $E_g = 2.13$  eV) for DCM in Ref. [73] is almost 1.4 times lower than our appreciated value from the DFT procedure in Table 3.

Tsuboi et al. [74] reported that one low absorption band and one intensive absorption band, respectively, for Znq<sub>2</sub> emerge at nearly 380 nm and 250 nm in acetonitrile solvent. Our especially measured ( $\lambda_{max} = 382$  nm) and computed ( $\lambda_{max} = 310.4$  nm) conclusions in the UV region for Znq<sub>2</sub> are fairly intimate to the evaluated results,  $\lambda_{max} = 380$  nm (our experimental data 382 nm with 2 nm discrepancies) and 250 nm (our simulation data 310.4 nm with 60 nm discrepancies), by Ref. [74]. It might be predicted that our other discrepancies on the rest of  $\lambda_{max}$  data for Znq<sub>2</sub> (347.5 nm measured and 433.7 nm simulated) compared to the published results (corresponding 250 and 380 nm, respectively) in Ref. [74] have been generated because of depending on solvent polarities of maximum absorption bands. Vergara et al. [75] operated the B3PW91/6-31G\*\* model chemistry to define the HOMO and LUMO of Znq<sub>2</sub> and discovered its HOMO-LUMO energy gap as 3.429 eV. Our computed outcome on HOMO-LUMO band gap in Table 3 for Znq<sub>2</sub> ( $E_g$  [HOMO-LUMO] = 3.49775 eV) is rather close to the derived value by Ref. [75]. The main nodal forms for HOMO and LUMO of Znq<sub>2</sub> are commanded by orbitals arising from the 8-hydroxy-quinoline ligands. The electrons intensities for HOMO and HOMO-1 of Znq<sub>2</sub> are condensed on the phenolate circles, while the LUMO and LUMO+1 are accommodated on the pyridyl fragments with fewer electron intensities than HOMO and HOMO-1, displaying similar MO distributions observed in Ref. [76].

**Table 4**Calculated maximum absorption wavelengths, oscillator strengths, and major compositions in terms of MO contributions for DCM and Znq<sub>2</sub>.

Compound	Excited state	Energy (eV)	Wavelength (nm)	Oscillator strength (f)	Major composition
DCM	1	2.8627	433.1	1.1065	HOMO→LUMO
	2	3.2292	383.9	0.0708	HOMO-1→LUMO
	3	3.7427	331.2	0.1088	HOMO-1→LUMO+1
	4	4.1342	299.9	0.2829	HOMO-1→LUMO
	5	4.1792	296.6	0.0637	HOMO→LUMO+1
Znq <sub>2</sub>	1	2.8586	433.7	0.0636	HOMO-1→LUMO
	2	2.8843	429.8	0.0091	HOMO→LUMO
	3	3.0320	408.9	0.0001	HOMO-1→LUMO+1
	4	3.0344	408.6	0.0001	HOMO-1→LUMO+1
	5	3.9931	310.4	0.0134	HOMO-1→LUMO+2

**Fig. 14.** Selected frontier molecular orbitals of DCM and Znq<sub>2</sub> calculated by DFT.

## 5. Conclusion

In this study, the structural and optical properties of thin films composed of DCM and Znq<sub>2</sub> with varying percentages of Znq<sub>2</sub> were investigated. The thin layers were deposited onto glass substrates using the physical vapor-phase deposition method under high vacuum

conditions. The surface morphology of the films was analyzed using Minkowski's functional analysis through the images obtained from atomic force microscopy (AFM). It was found that the addition of Znq<sub>2</sub> strongly influenced the morphology of the layers. The percentage of Znq<sub>2</sub> in the composition has an interesting dependence on the structure. As Znq<sub>2</sub> was present in abundance in the composition, its structure

dominated and eventually led to a structure similar to that of pure Znq<sub>2</sub>. On the other hand the TEM results revealed a consistent non-crystalline, amorphous structure in all samples, irrespective of the varying DCM percentages. This amorphous phase is a common feature of thin films deposited through Physical Vapor Deposition.

The doping of Znq<sub>2</sub> also affected the transmission spectra of the films. It was observed that even a small percentage of Znq<sub>2</sub> could increase the transmittance of the film, resulting in a decrease in absorbance. The Tauc plot method was used to determine the gap energies of the compounds through the transmittance spectra. Multiple gap values were identified in the thin films, with the films having different compositions showing the characteristic gap energies of pure DCM and pure Znq<sub>2</sub>, as well as two new bands. These results confirmed that a new structure was deposited with the combination of the two organic materials.

The FTIR spectroscopic analysis provides valuable insights into the composition of the thin films, confirming the presence of specific molecular groups associated with Znq<sub>2</sub> and DCM. The absence of unexpected peaks supports the conclusion that the thin films are of high purity, validating the deposition process and the reliability of the FTIR data for compositional determination.

Moreover, the DCM and Znq<sub>2</sub> organic semiconductor materials have been elaborated and efficiently characterized from UV–Vis spectral analysis. The geometries for title compounds have been optimized using the DFT approach. The resonance phenomena and several chemical reactions could be perceived with comprehension of the HOMO, LUMO and energy gap values for first and second frontier MOs. To search the CT properties of title molecules, the energy values on first and second frontier MOs have been ascertained by means of DFT. The HOMOs and LUMOs elucidated quite enough the molecular structure attributes for DCM and Znq<sub>2</sub>. Furthermore, in this work, the  $\lambda_{max}$  values of DCM and Znq<sub>2</sub> have been acquired computationally via TD-SCF/DFT. The simulated UV–Vis spectra and computed HOMO-LUMO gaps comply well enough with their corresponding measurement conclusions (UV–Vis) and data issued in the literature (UV–Vis and frontier MOs).

This study sheds light on the structural and optical properties of DCM films doped with different percentages of Znq<sub>2</sub> and their potential use in optoelectronic applications. The combination of experimental and theoretical approaches provided a comprehensive understanding of the materials, which help design and development of future devices.

#### CRediT authorship contribution statement

**Amina Laouid:** Writing – original draft, Investigation, Formal analysis, Data curation, Conceptualization. **Amine Alaoui Belghiti:** Supervision, Formal analysis. **Krzysztof Wisniewski:** Writing – review & editing, Supervision, Formal analysis. **Janusz Strzelecki:** Methodology, Investigation. **Asli Karakas:** Software, Methodology, Formal analysis. **Aysun Gozutok:** Software, Methodology, Formal analysis. **Youssef El kouari:** Investigation, Formal analysis. **Amal Bouich:** Formal analysis, Investigation, Methodology, Validation. **Mouhaydine Tlemçani:** Formal analysis, Investigation, Methodology. **Przemysław Płociennik:** Investigation, Formal analysis. **Abdelowahed Hajjaji:** Writing – review & editing, Validation, Supervision, Formal analysis. **Anna Zawadzka:** Supervision, Resources, Project administration, Investigation, Funding acquisition.

#### Declaration of competing interest

The authors declare that they have no known competing financial interests or personal relationships that could have appeared to influence the work reported in this paper.

#### Data availability

The authors do not have permission to share data.

#### Acknowledgements

This research has been financed from the funds of the Polish National Science Centre (grant no. 2017/25/B/ST7/02124). The films used in this paper were obtained using the Interdisciplinary Centre for Modern Technologies facilities, NCU, Toruń, Poland. The research was carried out as part of the IDUB project - emerging research fields: "Material Science and Technology". The author Amal Bouich acknowledges MCIN for funding support through Margarita Salas Fellowship (MCIN/AEI/10.13039/501100011033) and NextGenerationEU.

#### References

- [1] F. Bureš, Fundamental aspects of property tuning in push–pull molecules, RSC Adv. 4 (2014) 58826–58851, <https://doi.org/10.1039/C4RA11264D>.
- [2] T. Sano, Y. Nishio, Y. Hamada, H. Takahashi, T. Usuki, K. Shibata, Design of conjugated molecular materials for optoelectronics, J. Mater. Chem. 10 (2000) 157–161, <https://doi.org/10.1039/A903239H>.
- [3] F. Yang, S. Cheng, X. Zhang, X. Ren, R. Li, H. Dong, et al., 2D organic materials for optoelectronic applications, Adv. Mater. 30 (2018) 1702415, <https://doi.org/10.1002/adma.201702415>.
- [4] A. Franquet, V. Spampinato, S. Kayser, W. Vandervorst, P. van der Heide, Orbitrap™-SIMS analysis of advanced semiconductor inorganic structures, Vacuum 202 (2022) 111182, <https://doi.org/10.1016/j.vacuum.2022.111182>.
- [5] X.-L. Cao, S.-Y. Chen, X.-H. Huang, Controlling electron-spin filter via electric field in layered semiconductor nanostructure, Vacuum 206 (2022) 111541, <https://doi.org/10.1016/j.vacuum.2022.111541>.
- [6] Z. Abedi, M. Janghouri, E. Mohajerani, M. Alahbakhshi, A. Azari, A. Fallahi, Study of various evaporation rates of the mixture of Alq<sub>3</sub>: DCM in a single furnace crucible, J. Lumin. 147 (2014) 9–14, <https://doi.org/10.1016/j.jlumin.2013.10.020>.
- [7] M. Alcaire, L. Cerdán, F.L. Zamarro, F.J. Aparicio, J.C. González, F.J. Ferrer, et al., Multicolored emission and lasing in DCM-Adamantane Plasma Nanocomposite optical films, ACS Appl. Mater. Interfaces 9 (2017) 8948–8959, <https://doi.org/10.1021/acsami.7b01534>.
- [8] Z. Guo, W. Zhu, H. Tian, Dicyanomethylene-4H-pyran chromophores for OLED emitters, logic gates and optical chemosensors, Chem. Commun. 48 (2012) 6073–6084, <https://doi.org/10.1039/C2CC31581E>.
- [9] A. Mohamed, Studying the optical properties of thin films prepared from Polystyrene doped with DCM dye, Int. Lett. Chem. Phys. Astron. 61 (2015) 178–183, <https://doi.org/10.18052/www.scipress.com/ILCPA.61.178>.
- [10] J.-L. Bredas, J.R. Durrant, Organic photovoltaics, Acc. Chem. Res. 42 (2009) 1689–1690, <https://doi.org/10.1021/ar900238j>.
- [11] D. Mandal, S. Sen, K. Bhattacharyya, T. Tahara, Femtosecond study of solvation dynamics of DCM in micelles, Chem. Phys. Lett. 359 (2002) 77–82, [https://doi.org/10.1016/S0009-2614\(02\)00704-2](https://doi.org/10.1016/S0009-2614(02)00704-2).
- [12] Photophysical properties of 4-(dicyanomethylene)-2-methyl-6-(4-dimethylaminostyryl)-4H-pyran (DCM) and optical sensing applications | IntechOpen, n.d., <https://www.intechopen.com/chapters/72827>. (Accessed 4 September 2021).
- [13] A. Inoue, T. Hosokawa, M. Haishi, N. Ohtani, 4-(dicyanomethylene)-2-methyl-6-(p-dimethylaminostyryl)-4H-pyran (DCM)-doping density dependence of luminescence spectra and white emission in polymer light-emitting diodes, Phys. Status Solidi C 6 (2009) 334–337, <https://doi.org/10.1002/pssc.200879832>.
- [14] A. Laouid, A. Alaoui Belghiti, K. Wisniewski, A. Hajjaji, A. Zawadzka, Structural and optical properties of DCM thin films prepared by PVD, Mater. Today Proc. (2022), <https://doi.org/10.1016/j.mattpr.2022.03.244>.
- [15] A. Laouid, A.A. Belghiti, K. Wisniewski, A. Hajjaji, B. Sahraoui, A. Zawadzka, Generation of red light with intense photoluminescence assisted by Förster resonance energy transfer from Znq<sub>2</sub> and DCM thin films, Environ. Sci. Pollut. Res. (2022), <https://doi.org/10.1007/s11356-022-23217-z>.
- [16] S. Lee, M. Jen, Y. Pang, Twisted intramolecular charge transfer state of a “push–pull” emitter, Int. J. Mol. Sci. 21 (2020) 7999, <https://doi.org/10.3390/ijms21217999>.
- [17] A.Y. Mahmoud, K. Sulaiman, R.R. Bahabry, H. Alzahrani, Effect of donor on the performance of self-powered UV photodiodes based on solution-processed TPD: Alq<sub>3</sub> and NPD:Alq<sub>3</sub> active layers, Optik 244 (2021) 167538, <https://doi.org/10.1016/j.ijleo.2021.167538>.
- [18] J. Podlesný, O. Pytela, M. Klikar, V. Jelínková, V. Kitýk I, K. Ozga, et al., Small isomeric push–pull chromophores based on thiophenothenes with tunable optical (non)linearities, Org. Biomol. Chem. 17 (2019) 3623–3634, <https://doi.org/10.1039/C9OB00487D>.
- [19] S. Hashimoto, R. Takagi, K. Okamura, A. Yabushita, T. Kobayashi, I. Iwakura, Ultrafast charge transfer dynamics in the excited state of DCM measured by a 6-fs UV pulse laser, Chem. Phys. 551 (2021) 111326, <https://doi.org/10.1016/j.chemphys.2021.111326>.
- [20] M. Meyer, J.C. Mialocq, M. Rougée, Fluorescence lifetime measurements of the two isomers of the laser dye DCM, Chem. Phys. Lett. 150 (1988) 484–490, [https://doi.org/10.1016/0009-2614\(88\)87235-X](https://doi.org/10.1016/0009-2614(88)87235-X).
- [21] N. Kiseleva, D. Busko, B.S. Richards, M.A. Filatov, A. Turshatov, Determination of upconversion quantum yields using charge-transfer state fluorescence of heavy-

atom-free sensitizer as a self-reference, *J. Phys. Chem. Lett.* 11 (2020) 6560–6566, <https://doi.org/10.1021/acs.jpclett.0c01902>.

[22] C.-W. Chang, Y.-T. Kao, E.W.-G. Diau, Fluorescence lifetime and nonradiative relaxation dynamics of DCM in nonpolar solvent, *Chem. Phys. Lett.* 374 (2003) 110–118, [https://doi.org/10.1016/S0009-2614\(03\)00645-6](https://doi.org/10.1016/S0009-2614(03)00645-6).

[23] S.K. Pal, D. Mandal, D. Sukul, S. Sen, K. Bhattacharyya, Solvation dynamics of DCM in human serum albumin, *J. Phys. Chem. B* 105 (2001) 1438–1441, <https://doi.org/10.1021/jp0023680>.

[24] P.S. Choubey, N.N.S. Ojha, S. Ghosh, S.K. Varshney, B.N.S. Bhaktha, Origin of light scattering in dye doped polymeric waveguides and the dependence of excitation geometry on coherent random lasing, *J. Phys. Appl. Phys.* 53 (2020) 245104, <https://doi.org/10.1088/1361-6463/ab8039>.

[25] V. Jokanović, N. Bundaleski, B. Petrović, M. Ferarra, B. Jokanović, S. Živković, et al., Detailed physico-chemical characterization of the multilayered thin films based on titanium oxynitride and copper doped titanium nitride obtained by different PVD techniques, *Vacuum* 195 (2022) 110708, <https://doi.org/10.1016/j.vacuum.2021.110708>.

[26] B. Tili, C. Nouveau, M.J. Walock, M. Nasri, T. Ghrib, Effect of layer thickness on thermal properties of multilayer thin films produced by PVD, *Vacuum* 86 (2012) 1048–1056, <https://doi.org/10.1016/j.vacuum.2011.09.008>.

[27] V.P. Barberis, J.A. Mikroyannidis, Synthesis and optical properties of aluminum and zinc quinolates through styryl substituent in 2-position, *Synth. Met.* 156 (2006) 865–871, <https://doi.org/10.1016/j.synthmet.2006.05.007>.

[28] F. Jafari, S.M. Elahi, M.R. Jafari, A facile synthesis and optoelectronic characterization of Znq2 and Alq3 nano-complexes, *Appl. Phys. A* 124 (2018) 574, <https://doi.org/10.1007/s00339-018-1978-6>.

[29] M.R. Jafari, Z.S. Alirahmi, D. Ghanbari, Synthesis of CdSe and CdTe quantum dots: their effects on the Znq2 luminescence complex for organic light emitting diodes, *J. Nanostructures* 11 (2021) 153–164, <https://doi.org/10.22052/JNS.2021.01.017>.

[30] T. Tsuboi, Y. Nakai, Y. Torii, Photoluminescence of bis(8-hydroxyquinoline) zinc (Znq2) and magnesium (Mgq2), *Open Phys.* 10 (2012), <https://doi.org/10.2478/s11534-011-0090-8>.

[31] P. Shinde, S. Pandharipande, N. Thejkalyani, S.J. Dhole, Exploration of photophysical properties of green light emitting bis(8-hydroxyquinoline) zinc (Znq2) metal chelate under various environments, *Optik* 162 (2018) 151–160, <https://doi.org/10.1016/j.jleo.2018.02.075>.

[32] D. Painuly, R. Singhal, P. Kandwal, I.M. Nagpure, Structural, optical and decay properties of zinc(II) 8-hydroxyquinoline and its thin film, *J. Electron. Mater.* 49 (2020) 6096–6106, <https://doi.org/10.1007/s11664-020-08255-y>.

[33] A. Zawadzka, P. Płociennik, K. Waszkowska, Z. Masewicz, A. Aamoum, J. Strzelecki, et al., Physical Vapor Deposition technique and its application to thin organometallic films, in: 2017 19th Int. Conf. Transparent Opt. Netw. ICTON, IEEE, Girona, Spain, 2017, pp. 1–3, <https://doi.org/10.1109/ICTON.2017.8024901>.

[34] A. Zawadzka, P. Płociennik, J. Strzelecki, M. Pranaitis, S. Dabos-Seignon, B. Sahraoui, Structural and nonlinear optical properties of as-grown and annealed metallophthalocyanine thin films, *Thin Solid Films* 545 (2013) 429–437, <https://doi.org/10.1016/j.tsf.2013.07.042>.

[35] A. Zawadzka, K. Waszkowska, A. Karakas, P. Płociennik, A. Korcala, K. Wisniewski, et al., Diagnostic and control of linear and nonlinear optical effects in selected self-assembled metallophthalocyanine chlorides nanostructures, *Dyes Pigments* 157 (2018) 151, <https://doi.org/10.1016/j.dyepig.2018.04.048>.

[36] D. Nečas, P. Klapetek, Gwyddion: an open-source software for SPM data analysis, *Cent. Eur. J. Phys.* 10 (2012) 181–188, <https://doi.org/10.2478/s11534-011-0096-2>.

[37] A. Zawadzka, A. Marjanowska, P. Płociennik, A. Korcala, K. Wisniewski, B. Sahraoui, Properties and applications of hybrid organic-inorganic halide perovskites thin films, in: C.E. Tabor, F. Kajzar, T. Kaino (Eds.), *Org. Photonic Mater. Devices XXII*, SPIE, San Francisco, United States, 2020, p. 27, <https://doi.org/10.1117/12.2545957>.

[38] A.G. Korpi, Ş. Tülu, M. Bramowicz, A. Arman, S. Kulesza, B. Pszczołkowski, et al., Minkowski functional characterization and fractal analysis of surfaces of titanium nitride films, *Mater. Res. Express* 6 (2019) 086463, <https://doi.org/10.1088/2053-1591/ab26be>.

[39] P. Sanguino, M. Kunst, M. Ben Mbarek, M. Reghima, N. Bundaleski, O. Teodoro, et al., A contactless method to study carrier kinetics in SnS thin films, *Vacuum* 209 (2023) 111784, <https://doi.org/10.1016/j.vacuum.2022.111784>.

[40] H. Chfii, A. Bouich, A. Andrio, J.C. Torres, B.M. Soucase, P. Palacios, et al., The structural and electrochemical properties of CuCoO<sub>2</sub> crystalline nanopowders and thin films: conductivity experimental analysis and insights from density functional theory calculations, *Nanomaterials* 13 (2023) 2312, <https://doi.org/10.3390/nano13162312>.

[41] A.H. Aka, A. Bouich, B. Aka, B.M. Soucase, Synthesis and characterization of kesterite Cu<sub>2</sub>ZnSn(SxSe1-x)4 thin films with low-cost for efficient solar cells, *Results Opt.* 13 (2023) 100507, <https://doi.org/10.1016/j.rio.2023.100507>.

[42] H. chfii, A. Bouich, B. Mari Soucase, M. Abd-Lefdl, Structural and physical properties of Mg-doped CuCoO<sub>2</sub> delafossite thin films, *Mater. Chem. Phys.* 306 (2023) 128006, <https://doi.org/10.1016/j.matchemphys.2023.128006>.

[43] I. Solomon, M. Bhatnagar, K. Shukla, B. Sarma, M. Ranjan, A. Sarma, Correlation of structural and optical properties of PVD grown amorphous carbon thin films, *Diam. Relat. Mater.* 75 (2017) 69–77, <https://doi.org/10.1016/j.diamond.2017.01.015>.

[44] C. Degitz, M. Konrad, S. Kaiser, W. Wenzel, Simulating the growth of amorphous organic thin films, *Org. Electron.* 102 (2022) 106439, <https://doi.org/10.1016/j.orgel.2022.106439>.

[45] S. Fritze, C.M. Koller, L. von Fieandt, P. Malinovskis, K. Johansson, E. Lewin, et al., Influence of deposition temperature on the phase evolution of HfNbTiVZr high-entropy thin films, *Materials* 12 (2019) 587, <https://doi.org/10.3390/ma2040587>.

[46] M. Lougdali, M. Zazouli, Y. Abboud, A.E. Bouari, A. Zawadzka, P. Płociennik, et al., Linear and nonlinear optical properties of Manganese bis-(8-hydroxyquinoline) thin films for optoelectronic devices: experimental and computational studies, *J. Mol. Struct.* 1249 (2022) 131558, <https://doi.org/10.1016/j.molstruc.2021.131558>.

[47] R. Anoua, H. Lifi, S. Touhtouh, M. El Jouad, A. Hajjaji, M. Bakasse, et al., Optical and morphological properties of Curcuma longa dye for dye-sensitized solar cells, *Environ. Sci. Pollut. Res.* 28 (2021) 57860–57871, <https://doi.org/10.1007/s11356-021-14551-9>.

[48] J. Tauc, R. Grigorovici, A. Vancu, Optical properties and electronic structure of amorphous germanium, *Phys. Status Solidi B* 15 (1966) 627–637, <https://doi.org/10.1002/pssb.19660150224>.

[49] R. Shakoury, S. Rezaee, F. Mwema, C. Luna, K. Ghosh, S. Jurečka, et al., Multifractal and optical bandgap characterization of Ta<sub>2</sub>O<sub>5</sub> thin films deposited by electron gun method, *Opt. Quant. Electron.* 52 (2020) 95, <https://doi.org/10.1007/s11082-019-2173-5>.

[50] A. Escobedo-Morales, Ruiz-López II, M. deL. Ruiz-Peralta, L. Tepech-Carrillo, M. Sánchez-Cantú, J.E. Moreno-Orea, Automated method for the determination of the band gap energy of pure and mixed powder samples using diffuse reflectance spectroscopy, *Heliony* 5 (2019) e01505, <https://doi.org/10.1016/j.heliyon.2019.e01505>.

[51] B.D. Viezbicke, S. Patel, B.E. Davis, D.P. Birnie III, Evaluation of the Tauc method for optical absorption edge determination: ZnO thin films as a model system, *Phys. Status Solidi B* 252 (2015) 1700–1710, <https://doi.org/10.1002/pssb.201552007>.

[52] N. Fujii, Y. Ohmori, K. Yoshino, An organic infrared electroluminescent diode utilizing a phthalocyanine film, *IEEE Trans. Electron. Dev.* 44 (1997) 1204–1207, <https://doi.org/10.1109/16.605454>.

[53] K. Jung, Y. Kim, Theoretical studies of DCM derivatives with dual electron donating group, *Mol. Cryst. Liq. Cryst. - MOL CRYST. LIQ. CRYST.* 538 (2011) 45–52, <https://doi.org/10.1080/15421406.2011.563629>.

[54] L.M.A. Monzon, F. Burke, J.M.D. Coey, Optical, magnetic, electrochemical, and electrical properties of 8-hydroxyquinoline-based complexes with Al<sup>3+</sup>, Cr<sup>3+</sup>, Mn<sup>2+</sup>, Co<sup>2+</sup>, Ni<sup>2+</sup>, Cu<sup>2+</sup>, and Zn<sup>2+</sup>, *J. Phys. Chem. C* 115 (2011) 9182–9192, <https://doi.org/10.1021/jp201019c>.

[55] D. Painuly, N.K. Mogha, R. Singhal, P. Kandwal, D.T. Masram, M.E. Rabanal, et al., The modification in the photo-physical properties via transformation of synthetic dihydrated Znq2 to anhydrous (Znq2)4 tetramer by sublimation process, *Opt. Mater.* 82 (2018) 175–189, <https://doi.org/10.1016/j.optmat.2018.04.044>.

[56] M.E. Sánchez Vergara, L. Ramírez Vargas, C. Ríos, B. Molina, R. Salcedo, Investigation of structural and optoelectronic properties of organic semiconductor film based on 8-hydroxyquinoline zinc, *Electronics* 10 (2021) 117, <https://doi.org/10.3390/electronics10020117>.

[57] X. Wang, M. Shao, L. Liu, High photoluminescence and photoswitch of bis(8-hydroxyquinoline) zinc nanoribbons, *Synth. Met.* 160 (2010) 718–721, <https://doi.org/10.1016/j.synthmet.2010.01.008>.

[58] C. Engelter, G.E. Jackson, C.L. Knight, D.A. Thornton, Spectra-structure correlations from the infrared spectra of some transition metal complexes of 8-hydroxyquinoline, *J. Mol. Struct.* 213 (1989) 133–144, [https://doi.org/10.1016/0022-2860\(89\)85112-9](https://doi.org/10.1016/0022-2860(89)85112-9).

[59] S. Bakhshipour, Z. Shahedi, F. Mirahmadi, R. Fereidonnejad, M. Hesani, Effect of different in situ temperatures on the crystallinity and optical properties of green synthesized 8-hydroxyquinoline zinc by saffron extract, *Opt. Contin.* 1 (2022) 1401–1412, <https://doi.org/10.1364/OPTCON.459222>.

[60] Z. Wei, H. Song, C. Dai, Z. Chen, X. Yan, Z. Ji, et al., Tetramer bis(8-hydroxyquinoline) zinc crystals prepared by physical vapor deposition method, *Cryst. Res. Technol.* 52 (2017) 1700229, <https://doi.org/10.1002/crat.201700229>.

[61] S. Salam, S.M. Azooz, B. Nizamani, P.H.H. Zhang, A. Al-Masoodi, A. Mukhtar Diblaie, et al., A tunable-wavelength Q-switched fiber laser based on organic metal 8-hydroxyquinoline chelate as a saturable absorber, *Infrared Phys. Technol.* 131 (2023) 104637, <https://doi.org/10.1016/j.infrared.2023.104637>.

[62] D.C. Jung, Jong-Dal Hong, An organic nitrile dye with strong donor and acceptor groups for dye-sensitized solar cells, *Bull. Kor. Chem. Soc.* 32 (2011) 2083, <https://doi.org/10.5012/BKCS.2011.32.6.2083>.

[63] N. Tanigaki, H. Mochizuki, X. Mo, T. Mizokuro, T. Hiraga, T. Taima, et al., Molecular doping of poly(p-phenylenevinylene) under vacuum for photovoltaic application, *Thin Solid Films* 499 (2006) 110–113, <https://doi.org/10.1016/j.tsf.2005.07.032>.

[64] M.J. Frisch, et al., *Gaussian 03, Revision E.01*, Gaussian, Inc., Wallingford CT, 2004.

[65] R. Dennington, T. Keith, J. Millam, *GaussView, Version 5.0.9*, Semichem Inc., Shawnee Mission, KS, 2009.

[66] G. te Velde, F.M. Bickelhaupt, E.J. Baerends, C. Fonseca Guerra, S.J.A. van Gisbergen, J.G. Snijders, T. Ziegler, *Chemistry with ADF*, J. Comput. Chem. 22 (2001) 931–967.

[67] P.L. Franzen, S.C. Zilio, A.E.H. Machado, J.M. Madurro, A.G. Brito-Madurro, L.T. Ueno, R.N. Sampaio, N.M. Barbosa Neto, Experimental and theoretical investigation of first hyperpolarizability in aminophenols, *J. Mol. Struct.* 892 (2008) 254–260.

[68] C. Cardoso, P.E. Abreu, F. Nogueira, Structure dependence of hyperpolarizability in octopolar molecules, *J. Chem. Theor. Comput.* 5 (2009) 850–858.

[69] R. Anoua, S. Touhtouh, M. Rkhis, M. El Jouad, A. Hajjaji, F. Belhora, et al., Optical and electronic properties of the natural Alizarin dye: theoretical and experimental

investigations for DSSCs application, *Opt. Mater.* 127 (2022) 112113, <https://doi.org/10.1016/j.optmat.2022.112113>.

[70] M. Meyer, J.C. Mialocq, Ground state and singlet excited state of laser dye DCM: dipole moments and solvent induced spectral shifts, *Opt Commun.* 64 (3) (1987) 264–269.

[71] I.D. Petsalakis, D.G. Georgiadou, M. Vasilopoulou, G. Pistolis, D. Dimotikali, P. Argitis, G. Theodorakopoulos, Theoretical investigation on the effect of protonation on the absorption and emission spectra of two amine-group-bearing, red “push pull” emitters, 4-dimethylamino-4’-nitrostilbene and 4-(dicyanomethylene)-2-methyl-6-p-(dimethylamino) styryl-4H-pyran, by DFT and TDDFT calculations, *J. Phys. Chem. A* 114 (17) (2010) 5580–5587.

[72] Sena Hashimoto, Rikako Takagi, Kotaro Okamura, Atsushi Yabushita, Takayoshi Kobayashi, Izumi Iwakura, *Chem. Phys.* 551 (2021) 111326.

[73] F. Nüesch, D. Berner, E. Tutis, M. Schaer, C. Ma, X. Wang, B. Zhang, L. Zuppiroli, Doping-Induced charge trapping in organic light-emitting devices, *Adv. Funct. Mater.* 15 (2005) 323–330.

[74] Taiju Tsuboi, Yosuke Nakai, Yasuko Torii, *Cent. Eur. J. Phys.* 10 (2) (2012) 524–528.

[75] María Elena Sánchez Vergara, Lorena Ramírez Vargas, Citlalli Ríos, Bertha Molina, Roberto Salcedo, *Electronics* 10 (2021) 117.

[76] Linda S. Sapochak, Florencia E. Benincasa, Richard S. Schofield, Joseph L. Baker, K. Krystal, C. Riccio, Daniel Fogarty, Holger Kohlmann, Kim F. Ferris, Paul E. Burrows, *J. Am. Chem. Soc.* 124 (2002) 6119–6125.